The effect of dopants (Fe, Al) on the low-temperature activity and SO_2 tolerance in solvothermally synthesized MnO_x NH_3-SCR catalysts

Li, Huirong; Schill, Leonhard; Gao, Qi; Mossin, Susanne; Riisager, Anders

Published in:
Fuel

Link to article, DOI:
10.1016/j.fuel.2023.130111

Publication date:
2024

Document Version
Publisher's PDF, also known as Version of record

Fuel 358 (2024) 130111

Contents lists available at ScienceDirect

Fuel

journal homepage: www.elsevier.com/locate/fuel

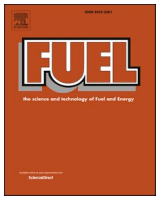

Full Length Article

The effect of dopants (Fe, Al) on the low-temperature activity and SO_2 tolerance in solvothermally synthesized MnO_x NH_3-SCR catalysts

Huirong Li, Leonhard Schill, Qi Gao, Susanne Mossin, Anders Riisager *

Centre for Catalysis and Sustainable Chemistry, Department of Chemistry, Technical University of Denmark, 2800 Kgs. Lyngby, Denmark

ARTICLE INFO

Keywords:
Low-temperature NH_3-SCR
Sulfur deactivation
Redox property
Electron transfer
Thermal regeneration

ABSTRACT

Fe-doped MnO_x catalyst prepared by a preferred solvothermal method displayed noticeably better low-temperature (LT) NH_3-SCR performance and water stability than an analogously prepared Al-doped MnO_x catalyst. The SCR activity of both catalysts decreased markedly when exposed to SO_2, but the resultant $MnFeO_x$-S catalyst retained higher LT activity than $MnAlO_x$-S and recovered significantly more of its original activity after thermal regeneration (400 °C). Comprehensive characterization confirmed that the deactivation of the catalysts was governed by formation of stable metal sulfates, which only decomposed to a minor extent upon thermal treatment although Al doping lowered the thermal stability of the adsorbed sulfur species. Additionally, Fe doping was found to facilitate electron transfer between Mn and Fe ions and weaken the interaction between active sites and deposited sulfates during the heating procedure, which promoted re-oxidation of Mn^{2+} to catalytically active Mn^{3+}/Mn^{4+}. Altogether, the altered redox properties resulted in improved LT SCR performance, enhanced water stability, higher SO_2 tolerance and superior regeneration of the $MnFeO_x$ catalyst.

1. Introduction

Nitrogen oxides (NO_x) are major atmospheric pollutants inducing a series of environmental problems like acid rain, photochemical smog, and ozone layer depletion [1]. Selective catalytic reduction of NO_x with NH_3 (NH_3-SCR) is considered the most effective approach for NO_x removal from stationary sources such as power- and incineration plants [2,3]. Traditionally V_2O_5-WO_3/TiO_2 (VWTi) catalysts are used for such installations, but recently low temperature (LT) NH_3-SCR catalysts have attracted considerable attention as these allow installing the SCR unit after flue gas desulfurization and dust removal units without the need for costly flue-gas reheating [4,5]. Particularly, environmentally benign Mn-based catalysts with excellent LT activity have been extensively studied as promising alternatives to VWTi catalysts. However, pure MnO_x catalysts suffer from a narrow active temperature window, undesirable NH_3 oxidation at relatively low temperature (>200 °C) and high sensitivity to water and SO_2 [6,7]. To overcome these drawbacks efforts have instead focused on modified catalysts containing MnO_x doped with other elements [8–10], MnO_x supported on other metal oxide supports [11,12], and Mn-containing materials with novel structures [13–16].

Fe is one of the most studied elements to modify MnO_x catalysts. Zhao et al. [17] doped different proportions of Fe species into Mn metal–organic frameworks (MOFs) and obtained upon different thermal treatments a series of MnO_x, Mn_4FeO_x, $MnFeO_x$ and $MnFe_4O_x$ catalysts. $MnFeO_x$ was found to have not only a large specific surface area but also good reduction ability and abundant oxygen vacancies, which all contributed to improved LT NH_3-SCR performance. In addition, the catalyst also showed better water resistance which the authors attributed to the significantly enhanced charge transfer between Fe and Mn species ($Mn^{4+} + Fe^{2+} \rightarrow Mn^{3+} + Fe^{3+}$, $Mn^{3+} + Fe^{2+} \rightarrow Mn^{2+} + Fe^{3+}$). Moreover, Wei et al. [18] reported a novel mesoporous nanostructured $Mn_{0.5}Fe_{2.5}O_4$ spinel catalyst with tailored redox properties. Its superior SCR catalytic activity was attributed mainly to appropriate redox properties derived from the unique structure with regularly dispersed active sites as well as preferentially exposed (220) crystal plane. Li et al. [19] further synthesized a series of $MnFeO_x$ nanorods with different Fe/Mn molar ratios, where $MnFe_{0.1}O_x$ showed the highest LT SCR performance as well as improved stability and resistance to water and SO_2. The concentration of surface chemisorbed oxygen and acid sites increased in the catalyst by the addition of Fe, and, more importantly, electronic transfer between Mn and Fe ions led to higher activity for oxidation of NO to NO_2. Hence, clearly the modification of Mn-based catalysts with Fe can benefit from both electronic and structural synergies.

* Corresponding author.
E-mail address: ar@kemi.dtu.dk (A. Riisager).

https://doi.org/10.1016/j.fuel.2023.130111
Received 15 August 2023; Received in revised form 5 October 2023; Accepted 13 October 2023
Available online 18 October 2023

Due to high thermal stability and acidic surface properties, alumina (Al_2O_3) is often used as a support to improve the catalytic activity of Mn-based catalysts. Jin et al. [20] supported Mn-Ce oxides on TiO_2 and Al_2O_3 and observed that Mn-Ce/Al_2O_3 exhibited a relatively higher SCR activity than Mn-Ce/TiO_2 above 150 °C due to more Brønsted acid sites. The higher acid density promoted adsorption and oxidation of NO to NO_2, and the consecutive reaction between NO_2/NO_2-containing species and adsorbed NH_3 led to higher NO conversion. Furthermore, Yao et al. [21] found MnO_x/γ-Al_2O_3 to exhibit the best LT NH_3-SCR performance, both in absence or presence of water and SO_2, when the influence of various supports on the catalytic performance of MnO_x was examined. This confirmed that Al_2O_3 also increased the SO_2 tolerance of MnO_x catalysts, and Fan et al. [22] explained this by facilitated decomposition of NH_4HSO_4 and lower thermal stability of adsorbed SO_2 species when Al_2O_3 was introduced into MnO_x. The abovementioned studies corroborate that introduction of Fe- and Al species to MnO_x catalysts increase SCR activity as well as the water and sulfur tolerance, but the promotion mechanisms remain more elusive. Additionally, a more direct comparison of the different promoting effects between Fe and Al has not been reported.

In this work, the impacts of water and SO_2 on the LT NH_3-SCR performance of $MnFeO_x$ catalysts synthesized by solvothermal method ($MnFeO_x$-H) and citric acid method ($MnFeO_x$-CA) are evaluated. $MnFeO_x$-H were shown to have the best tolerance for both water and SO_2. Subsequently, Al-doped $MnAlO_x$-H catalysts were also prepared and systematically examined to elucidate the effects of Fe and Al on the SCR performance, SO_2 resistance and catalyst regeneration. Appropriate characterization methods were further used to determine the impacts of the two metals on the poisoning and regeneration mechanism of the MnO_x catalysts.

2. Materials and methods

2.1. Catalyst preparation

$MnFeO_x$-H catalysts were prepared via a solvothermal method. In a typical procedure, an appropriate amount of manganese(III) acetylacetonate (≥99.0%, Sigma) and iron(III) acetylacetonate (≥97.0%, Sigma) (total amount of Mn and Fe was fixed at 2 mmol) were dissolved in a solution of 15 mL glycerol (≥98.0%, VWR) and 60 mL isopropanol (≥99.8%, VWR) at room temperature and stirred (500 rpm) for 30 min followed by ultrasonic treatment for 30 min. Then, the obtained mixture was transferred to a 200 mL sealed Teflon autoclave and maintained at 180 °C for 12 h. After cooling to room temperature, the product was collected and washed with deionized water (5 × 250 mL) and absolute ethanol (VWR) (2 × 100 mL) with intermediate centrifugation (12,000 rpm, 5 min) between each washing step. Finally, the product was dried at 100 °C overnight and calcined at 400 °C for 2 h in air with a heating rate of 2 °C/min. The obtained catalyst was denoted as $MnFeO_x$-H (x:y), where x:y refers to the molar ratio of Mn:Fe.

$MnAlO_x$-H catalysts were synthesized using the same solvothermal method as above with aluminum acetylacetonate (≥99.0%, Sigma) instead of iron(III) acetylacetonate, and denoted as $MnAlO_x$-H (x:y) with x:y referring to the molar ratio of Mn:Al. Likewise, pure MnO_x-H and FeO_x-H were also prepared by the same method without adding iron(III) acetylacetonate and manganese(III) acetylacetonate, respectively.

For comparison, $MnFeO_x$-CA (3:1) catalyst with the same elemental composition as $MnFeO_x$-H (3:1) was prepared according to a reported citric acid method [23]. The details are described in the Supporting Information.

Sulfur poisoned catalysts were obtained by pre-treating 100 mg of fractionized catalyst (45–60 mesh, 250–355 μm) in a fixed-bed quartz reactor with a gas flow of 100 ppm SO_2 + 4.5 vol% O_2/N_2 (100 mL/min) at 150 °C for 6 h (catalyst labeled with -S, e.g. $MnFeO_x$-S) to simulate the situation where only metal sulfates were present. Afterwards, the poisoned catalysts were treated at 400 °C for 2 h in static air, which is a normally used thermal regeneration method [22,24,25]. The obtained catalysts are labeled with -R, e.g. $MnFeO_x$-R.

2.2. Catalyst characterization

Transmission electron microscopy (TEM) was performed on a Tecnai T20 microscope equipped with an acceleration voltage of 200 kV. TEM samples were prepared by dispersing powder samples in ethanol with the aid of ultrasonic treatment for 5 min, followed by depositing droplets of the suspension on Lacey Carbon Films on 300 Mesh Copper Grids.

Elemental composition of samples was determined by scanning electron microscope (SEM) on a AFEG 250 Analytical ESEM equipped with an energy dispersive X-ray spectrometer (EDS) quanta 200FEG Oxford X-Max.

X-ray powder diffraction (XRD) was recorded on a Huber G670 powder diffractometer using Cu Kα radiation (λ = 1.5406 Å) within a 2θ range of 25–85°.

Nitrogen physisorption measurements were performed on a Micromeritics ASAP 2010 instrument at −196 °C after the sample was degassed at 110 °C for 24 h.

Thermogravimetric analysis (TGA) was done on a Mettler Toledo TGA/DSC 1 SF instrument from room temperature to 800 °C with a heating rate of 10 °C/min in N_2 flow (20 mL/min).

X-ray photoelectron spectroscopy (XPS) was carried out on a Thermo Scientific system at room temperature using Al Kα radiation (1484.6 eV) and a spot size of 400 μm equipped with a flood gun to reduce sample charging effects. All data were calibrated relative to the C 1s (284.8 eV).

Temperature-programmed reduction with H_2 (H_2-TPR) and temperature-programmed desorption of NH_3 (NH_3-TPD) were conducted on a Micromeritics Autochem-II instrument equipped with a thermal conductivity detector (TCD). Prior to H_2-TPR measurement, 50 mg sample was pre-treated in He flow (50 mL/min) at 200 °C for 3 h followed by cooling to 50 °C. Then, TCD signal was recorded from 50 to 800 °C at a rate of 10 °C/min in 5% H_2/Ar flow (50 mL/min). In a typical NH_3-TPD measurement the sample was pre-treated at 200 °C for 3 h and cooled to 100 °C, where after it was exposed to 1% NH_3/He (50 mL/min) for 1 h followed by purging with He (50 mL/min) at 100 °C for 30 min to remove weakly adsorbed NH_3. Finally, TCD signal was recorded from 50 to 600 °C at a rate of 10 °C/min in He flow (50 mL/min).

In-situ electron paramagnetic resonance (EPR) measurements were conducted using a Bruker X-band EMX EPR spectrometer equipped with a ST4102 cavity. The spectra were typically measured at a microwave frequency of 9.46 GHz with a modulation frequency of 100 kHz, modulation amplitude of 5.2 G and a time constant of 40.96 ms in the field range of 50 to 550 mT. Approximately 15 mg fractionized catalyst (45–60 mesh, 250–355 μm) was placed in an open-ended quartz tube and pretreated with 10 vol% O_2/He (200 mL/min) at 250 °C for 1 h followed by cooling to 200 °C under He (200 mL/min) before each measurement. After decreasing the temperature to 200 °C, the sample was exposed to different gas flows (200 mL/min), i.e. 1000 ppm NO + 1000 ppm NH_3/He for reduction, 1000 ppm NO + 10 vol% O_2/He for oxidation, 1000 ppm NO + 1000 ppm NH_3 + 10 vol% O_2/He for NH_3-SCR. EPR spectra were recorded every 1.6 min during the entire procedure.

2.3. Catalyst performance evaluation

NH_3-SCR activity measurements were generally performed with 50 or 100 mg of fractionized catalyst (45–60 mesh, 250–355 μm) in a fixed-bed quartz reactor (inner diameter 3.74 mm) using a feed gas containing 600 ppm NO, 600 ppm NH_3, 4.5 vol% O_2, 25 ppm SO_2 (when used), 2.5 vol% or 10 vol% H_2O (when used) with N_2 as balance at a fixed total gas flow rate of 200 mL/min (STP), corresponding to a weight hourly space velocity (WHSV) of 240,000 or 120,000 mL/g•h, respectively. However, for the determination of reaction kinetics (rate constant, *k*) 10 mg of fractionized catalyst (45–60 mesh, 250–355 μm) was used instead with a

high WHSV of 1,200,000 mL/g•h (STP) in the range of 60–100 °C, where the NO_x conversion was below 25%. Catalytic oxidation of NO and NH_3 were also measured in the same reactor setup using a feed gas containing 600 ppm NO or NH_3 and 4.75 vol% O_2 with N_2 as balance (WHSV 240,000 mL/g•h). Prior to measurement, each sample was pretreated at 200 °C for 30 min under 5 vol% O_2/N_2, followed by cooling to the starting temperature. This allowed to remove surface adsorbed impurities (like water), making the measurements fully reproducible.

The concentrations of the effluent gases NO, NO_2 and NH_3 from the reactor were in all experiments continuously monitored using a 17C NH_3 Analyzer (Thermo Electron Corporation) and recorded after reaching a steady state at each temperature (approx. 40 min). Meanwhile, N_2O at the outlet was measured by an Antaris IGS flue gas analyzer (Thermo Scientific, USA). The NO_x conversion (X), N_2 selectivity, NO to NO_2 conversion and NH_3 conversion were calculated as Eqs. (1)–(4), where $[NO_x]_{in}$, $[NO_2]_{in}$, $[NO]_{in}$ and $[NH_3]_{in}$ were the inlet concentrations of gaseous NO_x (including both NO and NO_2), NO_2, NO and NH_3, respectively. Likewise, $[NO_x]_{out}$, $[NO_2]_{out}$, $[NH_3]_{out}$ and $[N_2O]_{out}$ were the outlet concentrations of gaseous NO_x, NO_2, NH_3 and N_2O. The rate constant k (mL/g•s) was calculated as shown in Eq. (5) assuming a first-order reaction of NO and plug flow conditions, where F was the total flow rate (mL/s) at STP, W was the mass of catalyst (g), and X was the fractional NO_x conversion.

$$X(\%) = \frac{[NO_x]_{in} - [NO_x]_{out}}{[NO_x]_{in}} \times 100\% \quad (1)$$

$$N_2 \text{ selectivity } (\%) = \frac{[NO_x]_{in} - [NO_x]_{out} + [NH_3]_{in} - [NH_3]_{out} - 2[N_2O]_{out}}{[NO_x]_{in} - [NO_x]_{out} + [NH_3]_{in} - [NH_3]_{out}} \times 100\% \quad (2)$$

$$NO \text{ to } NO_2 \text{ conversion } (\%) = \frac{[NO_2]_{out} - [NO_2]_{in}}{[NO]_{in}} \times 100\% \quad (3)$$

$$NH_3 \text{ conversion } (\%) = \frac{[NH_3]_{in} - [NH_3]_{out}}{[NH_3]_{in}} \times 100\% \quad (4)$$

$$k = -\frac{F}{W} ln(1 - X) \quad (5)$$

3. Results and discussion

3.1. Catalyst performance

The performance of $MnFeO_x$-H catalysts with different Mn/Fe ratios was initially evaluated (Fig. S1a). $MnFeO_x$-H (3:1) having the same Mn/Fe ratio as previously reported optimal for a supported TiO_2 catalysts [26] was found to exhibit the highest SCR activity among all the $MnFeO_x$-H catalysts as well as pure MnO_x-H and FeO_x-H. Furthermore, the $MnFeO_x$-H (3:1) catalyst showed both improved water and SO_2 tolerance compared to the $MnFeO_x$-CA (3:1) catalyst prepared by citric acid method (Fig. S2). TEM images of $MnFeO_x$-H (3:1) revealed that the catalyst had a hybrid structure comprised of nanoparticles and nanotubes (Fig. S3a), whereas $MnFeO_x$-CA (3:1) consisted of only nanoparticles (Fig. S3b). Taking advantage of the hybrid structure, the influence of Al on the performance of $MnAlO_x$-H catalysts with different Mn/Al ratios was next evaluated. Here, $MnAlO_x$-H (2:1) with a similar hybrid structure (Fig. S3c) displayed higher LT NO_x conversion (<200 °C) than all the $MnAlO_x$-H catalysts as well as pure MnO_x-H (Fig. S1b), but its activity was lower than $MnFeO_x$-H (3:1) at all studied WHSVs (Fig. S4, $MnFeO_x$-H (3:1) and $MnAlO_x$-H (2:1) denoted briefly as $MnFeO_x$ and $MnAlO_x$, respectively). Notably, $MnFeO_x$ exhibited a broader temperature window and much higher rate constant value compared to those reported in literature (Table S1). In addition, both $MnFeO_x$ and $MnAlO_x$ exhibited a much higher N_2 selectivity than pure MnO_x (Fig. S5) with the latter showing the highest selectivity. This indicated clearly that both the loading of Fe and Al enhanced the N_2 selectivity of the MnO_x catalyst. In general, the $MnFeO_x$ catalyst ($\geq$ 90% NO conversion at 100–250 °C) had superior SCR performance (Fig. 1a) compared to the $MnAlO_x$ catalyst ($\geq$ 90% NO conversion at 150–250 °C).

The oxidation of NO to NO_2 has been reported to be beneficial for LT SCR by promoting "fast SCR" [10,27,28], and for this reason the NO oxidation ability of $MnFeO_x$ and $MnAlO_x$ were measured. As shown in Fig. 1b, $MnFeO_x$ yielded a higher NO oxidation rate than $MnAlO_x$ which could be responsible for the enhanced LT activity found in the SCR reaction (see above). On the other hand, NH_3 can also be unselectively oxidized to N_2 and N_2O especially at high temperatures, leading to a decrease of NO_x conversion and N_2 selectivity [29]. To check for this, the NH_3 oxidation activity was evaluated for the two catalysts (Fig. 1c). For both catalysts, the NH_3 conversion increased with temperature reaching around 68% ($MnAlO_x$) and 89% ($MnFeO_x$) at 200 °C, thus corroborating that undesired oxidation was an important factor for the observed decrease of SCR catalytic activity above 200 °C and the lower N_2 selectivity of $MnFeO_x$ compared to that of $MnAlO_x$ (Fig. S5).

Kinetic experiments were further carried out with the two catalysts at relatively high WHSV (1,200,000 mL/g•h) in the temperature range of 60–100 °C (NO_x conversions < 25%). Arrhenius plots based on the first-order rate constants of the two catalysts are shown in Fig. 1d along with the corresponding apparent activation energies (E_a) and pre-exponential factors (A). $MnFeO_x$ exhibited the highest reaction rate despite the higher E_a (53.6 ± 1.5 kJ/mol) compared to $MnAlO_x$ (41.4 ± 2.3 kJ/mol). This is reasonable because the A value was found to be two orders of magnitude larger for $MnFeO_x$ than for $MnAlO_x$, thus indicating a much higher reaction probability of the former catalyst due to a higher density of catalytically active sites.

3.2. Effects of H_2O and SO_2 on catalyst performance

In practical applications, flue gas often contains a significant moisture content and the performance of $MnFeO_x$ and $MnAlO_x$ was therefore assessed at 185 °C with the presence of 10 vol% H_2O in the feed gas (Fig. S6a). Before the introduction of H_2O, the two catalysts exhibited stable activity with NO conversion levels of 95 and 91%, respectively. Upon H_2O exposure the conversions declined within the first 2 h before stabilizing at 55 and 37%, respectively, indicating greater water tolerance of $MnFeO_x$. However, after removing H_2O from the feed gas both catalysts recovered almost completely their initial activity, thus demonstrating that the water-induced inhibition was reversible. Conversely, the N_2 selectivity of both catalysts increased after introducing H_2O to the feed gas (Fig. S6b), suggesting that H_2O had a strong inhibition on N_2O formation during the LT SCR reaction, consistent with previous studies [7,30].

SO_2 is another important component in real flue gas. To assess the SO_2 tolerance of the $MnFeO_x$ and $MnAlO_x$ catalysts, an initial test was conducted by continuously introducing SO_2 (25 ppm) into the feed gas at 185 °C (Fig S7). The results confirmed that both catalysts exhibited a significant reduction in NO_x conversion over time, and thus limited tolerance to SO_2 as also found for other Mn-based catalysts [6,7]. However, $MnFeO_x$ displayed a slower deactivation rate compared to $MnAlO_x$, suggesting a higher SO_2 tolerance of the former catalyst.

The primary cause of irreversible deactivation of Mn-based SCR catalysts has been shown to be the formation of metal sulfates (mainly $MnSO_4$), exhibiting limited thermal decomposition within the operating temperature range [24,31]. To clarify the impact of these sulfates on the performance of the Fe/Al-doped MnO_x catalysts, an activity evaluation and comparison was performed among fresh $MnFeO_x$ and $MnAlO_x$ catalysts, the respective S-poisoned catalysts obtained through pretreatment with SO_2, and thermally regenerated catalysts (Fig. 2a-c). The NO_x conversion with both S-poisoned catalysts decreased significantly at low temperatures, but $MnFeO_x$-S maintained a much higher activity than

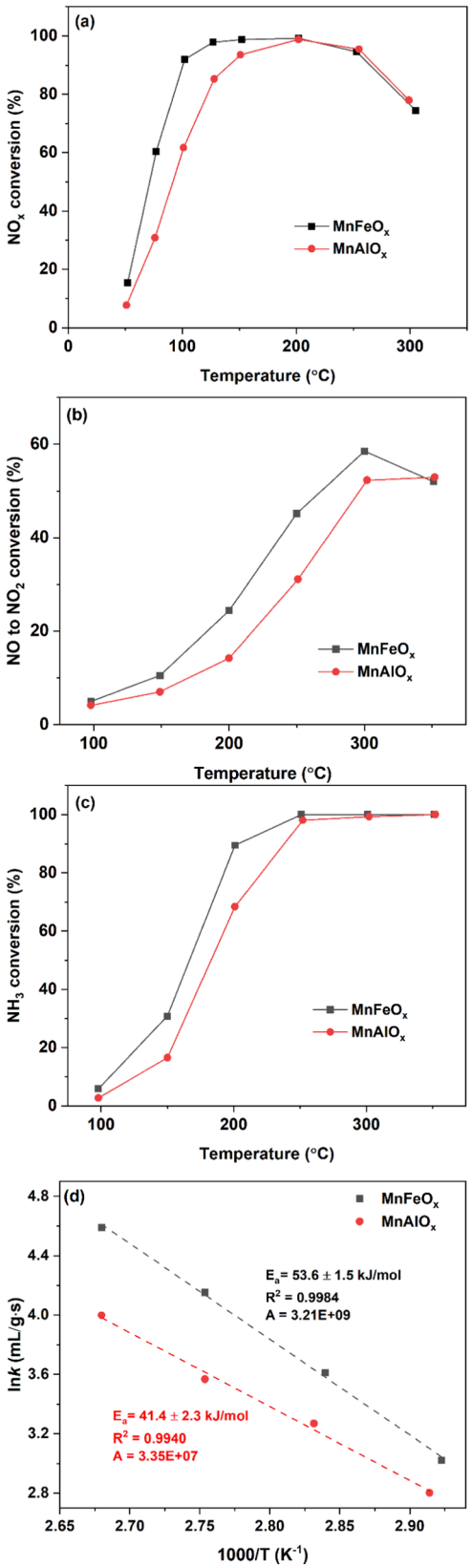

Fig. 1. (a) NO_x conversion, (b) NO to NO_2 conversion, and (c) NH_3 conversion of $MnFeO_x$ and $MnAlO_x$ as well as (d) Arrhenius plots based on the reaction rate constants of $MnFeO_x$ and $MnAlO_x$ between 60 and 100 °C. Reaction conditions: [NO] = 600 ppm (a and b), [NH_3] = 600 ppm (a and c), [O_2] = 4.5 vol%, balanced by N_2, WHSV = 240,000 mL/g·h (a-c) and 1,200,000 mL/g•h (d).

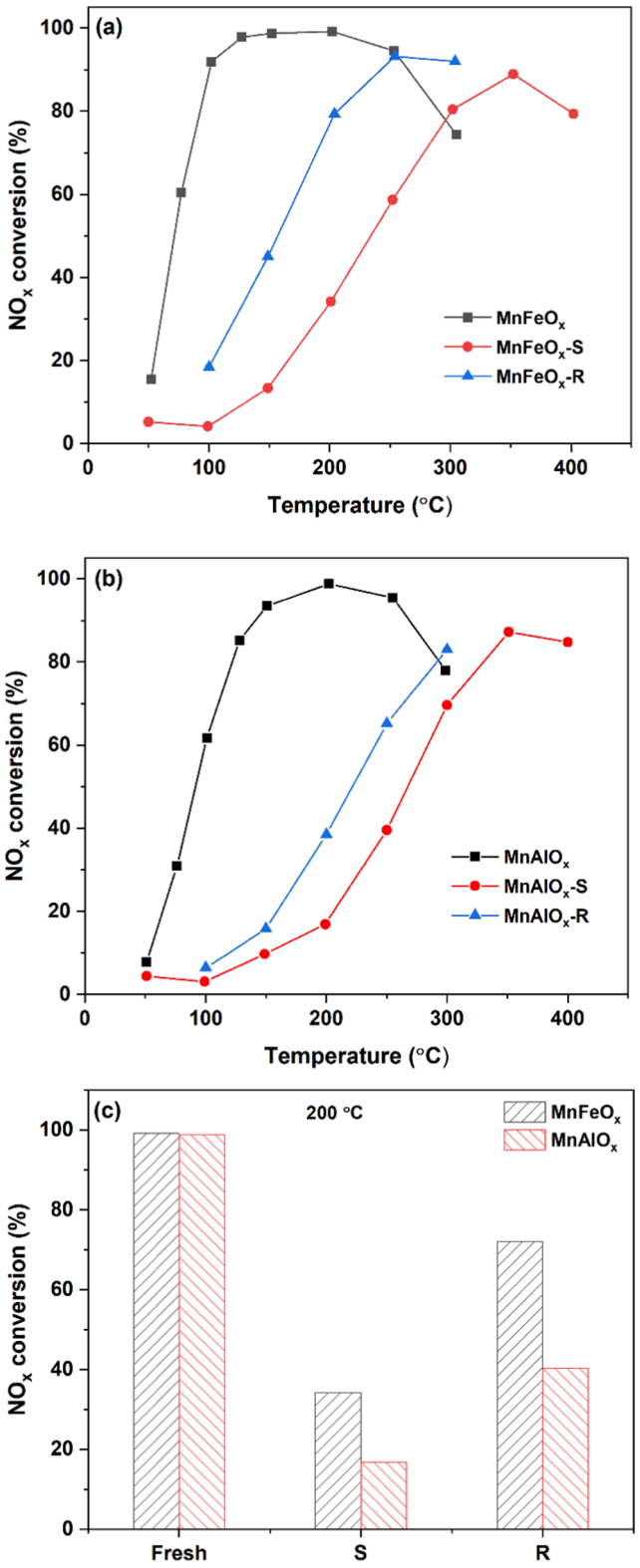

Fig. 2. NO_x conversion during NH_3-SCR of fresh (Fresh), poisoned (S) and thermally regenerated (R) (a) $MnFeO_x$ and (b) $MnAlO_x$ catalyst. (c) Comparison of the NO_x conversions of the different catalysts at 200 °C. Reaction conditions: [NO] = [NH_3] = 600 ppm, [O_2] = 4.5 vol%, balanced by N_2, WHSV = 240,000 mL/(g·h).

$MnAlO_x$-S at ≥ 150 °C yielding higher NO_x conversion, e.g. 34% ($MnFeO_x$-S) and 17% ($MnAlO_x$-S) at 200 °C. After thermal regeneration, the activity of $MnFeO_x$-R was well recovered and even higher than the fresh sample at 300 °C (likely due to less unselective NH_3 oxidation). Oppositely, the activity of $MnAlO_x$-R restored only to a lesser extent confirming that $MnFeO_x$ exhibited both stronger SO_2 resistance and better thermal recoverability than $MnAlO_x$.

3.3. Composition and morphology of catalysts

To reveal the factors contributing to the different performance obtained for the $MnFeO_x$ and $MnAlO_x$ catalysts, a series of characterization experiments were carried out. The composition of catalysts obtained from SEM-EDS mapping (Figs. S8 and S9) and listed in Table 1 showed that the atomic ratios of Fe/Mn (0.37) and Al/Mn (0.53) in the fresh samples were close to the theoretical values of 0.33 and 0.50, respectively. Moreover, no obvious difference in sulfur concentration among the S-poisoned and thermally regenerated catalysts was observed, but the surface atomic ratios of Fe/Mn and Al/Mn calculated from XPS (Table 2, see Section 3.4) were much higher than those found by SEM-EDS analysis. In combination with XRD analysis of $MnFeO_x$ and $MnAlO_x$ (Fig. 3) where peaks corresponding to Fe_2O_3 and Al_2O_3, but not MnO_x species, were observed, this suggested that Fe and Al mainly aggregated on the surface and that their doping improved the dispersion of MnO_x species. Moreover, after sulfur poisoning the XRD diffraction peaks of Fe_2O_3 and Al_2O_3 were much weakened. However, for $MnAlO_x$-R the Al_2O_3 peaks reappeared after regeneration indicating that species of weakly adsorbed SO_2 on Al_2O_3 decomposed during the thermal treatment [22]. This also matched well with the XPS results where the Al/Mn ratio was found to increase after thermal regeneration (Table 2). Also, the large relative difference of surface sulfur concentration before and after thermal regeneration (19%) indicated formation of less stable surface sulfur species on $MnAlO_x$-S.

TGA measurements were performed to examine the generated sulfur species on the S-poisoned and thermally regenerated catalysts in more detail (Fig. 3c). The weight losses of all catalysts could be assigned to desorption of physically adsorbed water and impurities (step I, < 200 °C), loss of weakly adsorbed surface sulfur species (step II, 200–400 °C) and release of O_2 from metal oxides and decomposition of more stable metal sulfates, e.g. manganese sulfate and iron sulfate (step III, > 400 °C) [22,25,32,33]. For the $MnFeO_x$-S catalyst the weight loss in step II and step III were 3.3 and 9.7% respectively, while they were 4.7 and 9.8% for the $MnAlO_x$-S catalyst. After thermal regeneration at 400 °C, the weight loss of $MnFeO_x$-R and $MnAlO_x$-R in step II were 3.0 and 4.0%, respectively, thus revealing a relatively larger weight loss between poisoned/regenerated catalysts for $MnAlO_x$ (0.7%) than for $MnFeO_x$ (0.3%). This suggested formation of more weakly adsorbed surface sulfur species (mainly $Al_2(SO_4)_3$) in the former catalyst system, which is in line with other studies where introduction of Al_2O_3 to MnO_x has been found to reduce the thermal stability of adsorbed sulfur species [22]. On the other hand, the weight losses in step III for the regenerated catalysts were higher ($MnFeO_x$-R: 10.9%, $MnAlO_x$-R: 10.1%) than that of the poisoned samples, which may be due to the release of oxygen from higher valence state metal oxides formed during the thermal regeneration process.

The specific surface area and porosity of the different $MnFeO_x$ and $MnAlO_x$ catalysts were further analyzed by N_2 physisorption (Fig. S10), which showed that all catalysts exhibited type IV isotherms with H3 type hysteresis indicative of mesoporous structures. The surface area and pore volume of the fresh catalysts were reduced to less than half after sulfur poisoning, while the average pore size increased slightly (Table 1). This indicated coverage of the surface by metal sulfates and possible blockage of small pores, which could be important factors for the deactivation as larger surface area usually corresponds to more active sites and higher catalytic activity. However, as fresh $MnAlO_x$ had a larger surface area than fresh $MnFeO_x$ but lower LT SCR activity, other factors than the surface area contributed to the activity difference between the catalyst systems.

3.4. Surface elemental states in catalysts

XPS analyses were performed with the different $MnFeO_x$ and $MnAlO_x$ catalysts to determine surface chemical compositions and elemental states. The Mn 2p XPS spectra of the fresh catalysts (Figs. 4a and b) revealed three peaks corresponding to Mn^{2+} (640.5 eV), Mn^{3+} (641.6–641.7 eV) and Mn^{4+} (643.1–643.5 eV), while the S-poisoned and thermally regenerated catalysts gave peaks assigned to Mn^{2+} (639.9–640.4 eV), Mn^{3+} (641.6–642.2 eV) and Mn^{4+} (643.9–644.3 eV), respectively [34]. The two latter peaks were shifted to higher binding energies, which could be due to the stronger electron-withdrawing effect of sulfate species compared to that of oxide ions, thus making the binding energies of neighboring Mn^{3+} and Mn^{4+} species shift to higher energies [35,36]. After thermal regeneration, all peaks in $MnFeO_x$-R were moved to lower binding energies while those from $MnAlO_x$-R remained almost unchanged, thus indicating that a weakened combination between Mn and SO_4^{2-} occurred mainly in the $MnFeO_x$-R catalyst after the heating.

The relative atomic ratios of Mn^{4+}, Mn^{3+} and Mn^{2+} in all catalysts were calculated from the integrated peak areas (Table 2). The Mn^{4+} ratio in fresh $MnFeO_x$ (31.5%) was higher than that in fresh $MnAlO_x$ (28.2%), possibly explaining the catalyst's higher NO oxidation activity as Mn^{4+} has been reported to favor the oxidation of NO to NO_2 [8,37]. After SO_2 poisoning, the Mn^{4+} ratios in both catalysts decreased markedly and was only partly recovered by thermal regeneration (likely re-oxidation of Mn^{2+} to Mn^{4+}). Oppositely, the Mn^{2+} ratios in $MnFeO_x$-S (18.8%) and $MnFeO_x$-R (8.4%) were lower than those in $MnAlO_x$-S (23.3%) and $MnAlO_x$-R (20.0%), especially after regeneration, which could be ascribed to re-oxidation of Mn^{2+} through redox cycles between $Mn^{4+}/Mn^{3+}/Mn^{2+}$ and Fe^{3+}/Fe^{2+} [17,19]. Previous studies have demonstrated that Mn species in higher oxidation states are conducive to redox reactions over Mn-based catalysts [9,38], and the higher fractions of Mn^{4+} and Mn^{3+} in $MnFeO_x$-S and $MnFeO_x$-R may therefore play an important role for their higher relative LT SCR activity.

In the Fe 2p XPS spectra of $MnFeO_x$, $MnFeO_x$-S and $MnFeO_x$-R (Fig. 4c), two main peaks assigned to Fe $2p_{3/2}$ (710 eV) and Fe $2p_{1/2}$ (724 eV) [39,40] could be deconvoluted into Fe^{3+} and Fe^{2+} [23] and

Table 1
Composition and pore structure of catalysts.

Catalyst	Element conc. (wt%)[a]				Atomic ratio[a]		Surface area (m^2/g)[b]	Pore volume (cm^3/g)[b]	Average pore size (nm)[b]
	Mn	Fe	Al	S	Fe/Mn	Al/Mn			
$MnFeO_x$	54.8	20.8	–	–	0.37	–	132.0	0.20	6.08
$MnFeO_x$-S	45.7	17.8	–	4.3	0.38	–	62.6	0.11	7.06
$MnFeO_x$-R	42.9	16.7	–	4.4	0.38	–	54.8	0.10	7.18
$MnAlO_x$	48.5	–	12.6	–	–	0.53	163.5	0.30	7.45
$MnAlO_x$-S	49.3	–	9.9	3.8	–	0.41	64.0	0.16	10.10
$MnAlO_x$-R	47.2	–	11.3	4.1	–	0.49	75.2	0.18	9.33

[a] Determined by SEM-EDS mapping. [b] Determined by N_2 physisorption.

Table 2
Surface composition and elemental atomic ratios in catalysts.

Catalyst	Surface composition (atomic %) and atomic ratio[a]							Relative atomic ratio (%)[a,b]							
	Mn	Fe	Al	O	S	Fe/Mn	Al/Mn	Mn^{2+}	Mn^{3+}	Mn^{4+}	Fe^{2+}	Fe^{3+}	O_α	O_β	O_γ
$MnFeO_x$	24.6	13.2	–	62.2	–	0.54	–	3.4	65.1	31.5	61.5	38.5	57.5	42.5	–
$MnFeO_x$-S	20.6	12.1	–	64.5	2.7	0.59	–	18.8	64.0	17.2	80.6	19.4	22.2	32.6	45.2
$MnFeO_x$-R	20.9	10.2	–	66.4	2.5	0.49	–	8.4	70.5	21.1	76.9	23.1	19.5	40.7	39.8
$MnAlO_x$	20.8	–	15.5	63.8	–	–	0.75	5.2	66.6	28.2	–	–	56.5	43.5	–
$MnAlO_x$-S	15.3	–	14.3	66.2	4.2	–	0.94	23.3	58.6	18.1	–	–	25.0	27.0	48.0
$MnAlO_x$-R	16.3	–	17.6	62.6	3.4	–	1.08	20.0	57.3	22.7	–	–	23.6	32.0	44.4

[a] Determined by XPS. [b] Calculated as $Mn^{2+}/(Mn^{4+} + Mn^{3+} + Mn^{2+})$, $Mn^{3+}/(Mn^{4+} + Mn^{3+} + Mn^{2+})$, $Mn^{4+}/(Mn^{4+} + Mn^{3+} + Mn^{2+})$, $Fe^{3+}/(Fe^{3+} + Fe^{2+})$, $Fe^{2+}/(Fe^{3+} + Fe^{2+})$, $O_\alpha/(O_\alpha + O_\beta + O_\gamma)$, $O_\beta/(O_\alpha + O_\beta + O_\gamma)$ and $O_\gamma/(O_\alpha + O_\beta + O_\gamma)$, respectively.

their relative atomic ratio calculated (Table 2). The Fe^{3+} ratio decreased significantly after poisoning (38.5 to 19.4%) due to reduction by SO_2. However, upon thermal regeneration the Fe^{3+} ratio increased again to some extent (23.1%), possibly due to the abovementioned redox reactions between Mn- and Fe species. Moreover, the Fe^{3+} peak was shifted to higher binding energy after poisoning but to lower energy after thermal regeneration, indicating that the bonding between SO_4^{2-} and Fe^{3+} was weakened by the thermal regeneration process. The change of chemical environment of Fe^{3+} was in accordance with the change found for Mn, confirming that heating promoted the electron transfer between Mn and Fe which weakened the interactions of both Mn and Fe^{3+} with SO_4^{2-}.

Likewise, in the O 1s XPS spectra of the SO_2 poisoned and regenerated catalysts (Fig. 4d) three peaks could be assigned to lattice oxygen O_α (529.0–529.4 eV), surface chemisorbed oxygen O_β (530.0–530.9 eV), and physisorbed water O_γ (531.2–532.2 eV) associated to the surface metal sulfates, respectively [41]. It has been reported that O_β plays a more important role than O_α and O_γ for the SCR activity of Mn catalysts due to its higher mobility [37,42,43]. In line with this, the O_β ratios for $MnFeO_x$-S (32.6%) and $MnFeO_x$-R (40.7%) were much higher than that of $MnAlO_x$-S (27.0%) and $MnAlO_x$-R (32.0%), leading to the better catalytic activity shown in Fig. 2.

3.5. Redox properties of catalysts

H_2-TPR was performed to reveal redox properties of the different $MnFeO_x$ and $MnAlO_x$ catalysts, as lower reduction temperatures of catalytically active species correlate with stronger ability to oxidize NO to NO_2 and better LT NH_3-SCR [44,45]. For the fresh $MnFeO_x$ catalyst (Fig. 5a), a peak centered at 273 °C was attributed to the reduction of MnO_2 to Mn_2O_3 whereas two other peaks at 399 °C and 586 °C were ascribed to overlapping reduction of Fe_2O_3 to Fe_3O_4/Mn_2O_3 to MnO and the reduction of Fe_3O_4 to FeO, respectively [9,39,44,46]. In $MnFeO_x$-S, a strong peak appeared at 495 °C and the intensity of the second reduction peak increased significantly due to the coupled reduction of Mn^{3+} and SO_4^{2-} [47,48]. In addition, the first peak shifted to a higher temperature (370 °C) indicating the strong metal-sulfate interaction between Mn and SO_4^{2-} and lower redox ability of the $MnFeO_x$-S catalyst. After heat treatment, all peaks shifted to lower temperatures suggesting that the redox ability of $MnFeO_x$-R was restored to some extent and confirmed that Mn/Fe and SO_4^{2-} interactions were weakened in accordance with the XPS results (see above). For all the catalysts were the reduction peaks fitted (Fig. S11) and the peak positions (Peak I: MnO_2 to Mn_2O_3, Peak II: Mn_2O_3 to MnO) as well as the H_2 consumptions calculated by the peak areas listed in Table S2. The H_2 consumption (Peak I + II) of $MnFeO_x$-R was much higher than that of $MnFeO_x$-S, indicating more reducible Mn sites in the latter catalyst.

In the H_2-TPR profile of the fresh $MnAlO_x$ catalyst (Fig. 5b), two reduction peaks ascribed to Mn^{4+}/Mn^{3+} (291 °C) and Mn^{3+}/Mn^{2+} (444 °C) were also seen. In the same way, sulfur poisoning had similar effects on the redox property of $MnAlO_x$-S, i.e. both peaks were shifted to higher temperatures and the intensity of the second peak increased significantly due to the overlapped reduction of Mn^{3+} and SO_4^{2-}. Similarly, the first reduction peak was shifted to slightly lower temperature for the $MnAlO_x$-R catalyst after regeneration, but to a much smaller extent than that of $MnFeO_x$-R. In addition, the difference of H_2 consumption between $MnAlO_x$-S and $MnAlO_x$-R was much smaller than that between $MnFeO_x$-S and $MnFeO_x$-R (Table S2), indicating a lower recoverability of reducible Mn sites over $MnAlO_x$ compared to $MnFeO_x$. Overall, the $MnAlO_x$ catalysts were generally reduced at higher temperatures than the corresponding $MnFeO_x$ catalysts, and this lower reducibility was likely a main reason why the $MnAlO_x$ catalysts exhibited inferior SCR performance in comparison to the $MnFeO_x$ catalysts.

3.6. Acidity of catalysts

NH_3-TPD measurements were carried out on the different $MnFeO_x$ and $MnAlO_x$ catalysts (Fig. S12) to investigate their acid properties, as both the density and strength of acid sites are important for the SCR reaction [34,49]. NH_3 adsorbed on weak acid sites can generally be activated at lower temperature and therefore be beneficial for LT SCR, while NH_3 adsorbed on medium and strong acid sites contributes only at relatively high temperatures [22]. $MnFeO_x$ (Fig. S12a) exhibited in the temperature range 100–350 °C one desorption peak at 162 °C attributed to NH_3 adsorbed on weak acid sites (0.33 mmoL/g). After SO_2 poisoning, the amount of adsorbed NH_3 was significantly increased and a new peak at 285 °C ascribed to medium-strong acid sites appeared for $MnFeO_x$-S [50], which could be due to abundant Brønsted acid sites resulting from the formation of SO_4^{2-} after poisoning [48,51,52]. This confirmed that the poisoning resulted in both higher acid density (1.29 mmoL/g) and acid site strength. After thermal regeneration, the density of the medium-strong acid sites was lowered in $MnFeO_x$-R due to partial decomposition of the surface sulfates, but the NH_3 adsorption and acid density (0.78 mmoL/g) remained much higher than that of the fresh catalyst.

The $MnAlO_x$ catalysts exhibited similar NH_3-TPD peaks and trends as $MnFeO_x$ between fresh, poisoned and regenerated catalysts (Fig. S12b) resulting in acid sites densities of $MnAlO_x$ (0.49 mmoL/g), $MnAlO_x$-S (1.32 mmoL/g) and $MnAlO_x$-R (1.18 mmoL/g), respectively. Considering the SCR activity results (Fig. 2) where the Fe-doped catalysts exhibited better LT performance than the Al-doped catalysts, it is therefore clear that the surface acidity was not a main factor contributing to the observed activity difference.

3.7. In-situ EPR of catalysts

The difference in redox ability of the $MnFeO_x$ and $MnAlO_x$ catalysts was above corroborated to be a main factor responsible for the different catalytic behavior of the catalysts. To provide further insight on the redox abilities *in-situ* EPR measurements was performed on the catalysts during exposure to various feed gases, i.e. NH_3/NO, O_2/NO and NH_3/NO/O_2 at 200 °C. $MnFeO_x$ showed after pretreatment (O_2/He at 250 °C for 1 h followed by cooling to 200 °C in He) a small EPR signal at $g_\perp =$

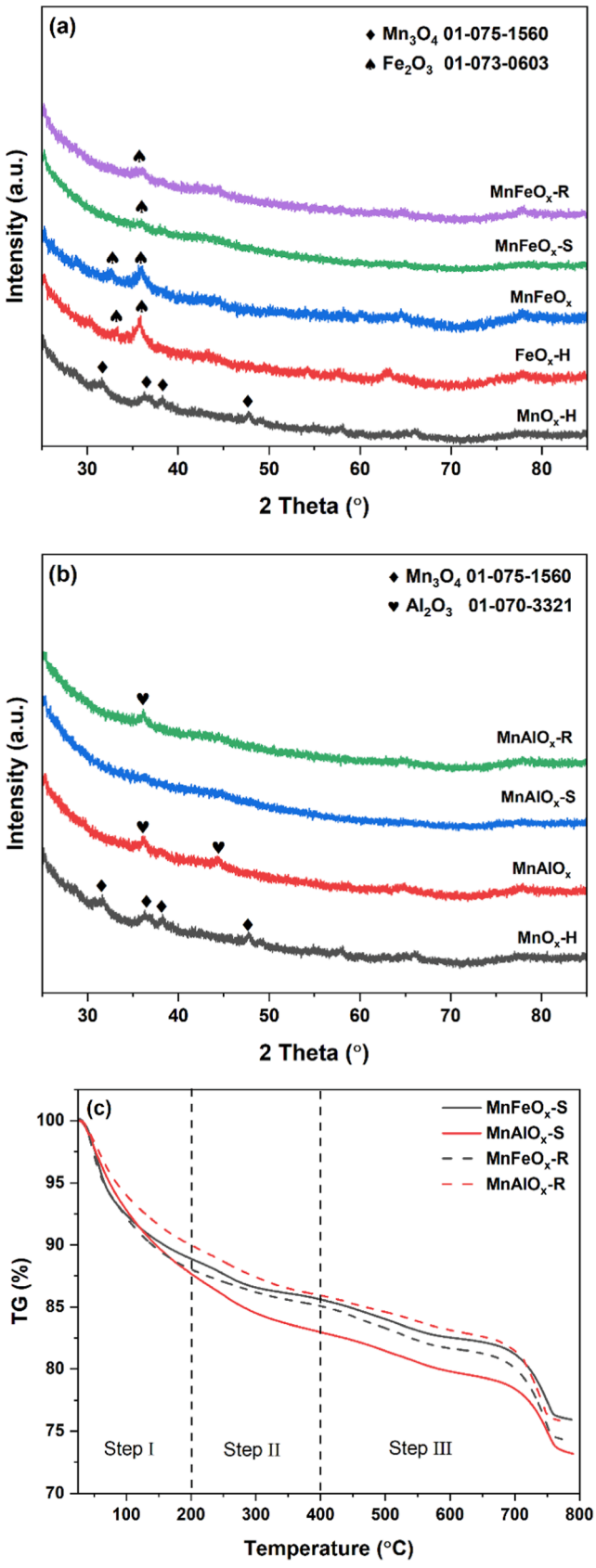

Fig. 3. XRD patterns of fresh, poisoned (S) and thermally regenerated (R) (a) $MnFeO_x$ and (b) $MnAlO_x$ catalysts along with reference materials. (c) TG profiles of poisoned (S) and thermally regenerated (R) $MnFeO_x$ and $MnAlO_x$ catalysts.

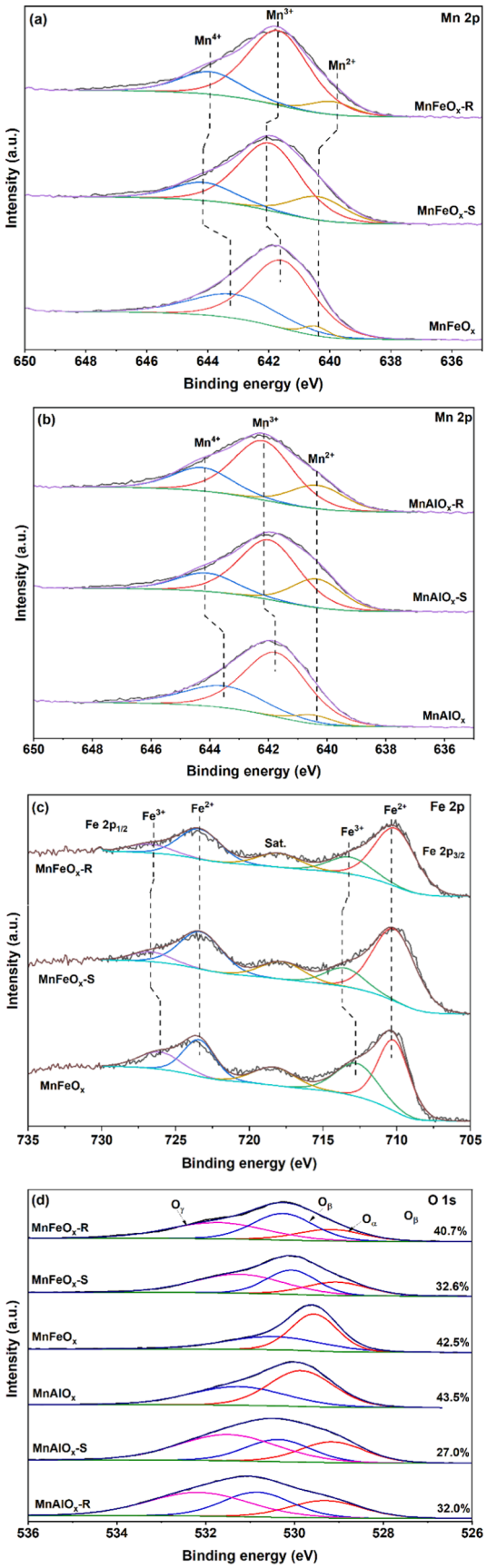

Fig. 4. (a) and (b) Mn 2p, (c) Fe 2p, and (d) O 1s XPS spectra of fresh, poisoned (S) and thermally regenerated (R) $MnFeO_x$ and $MnAlO_x$ catalysts.

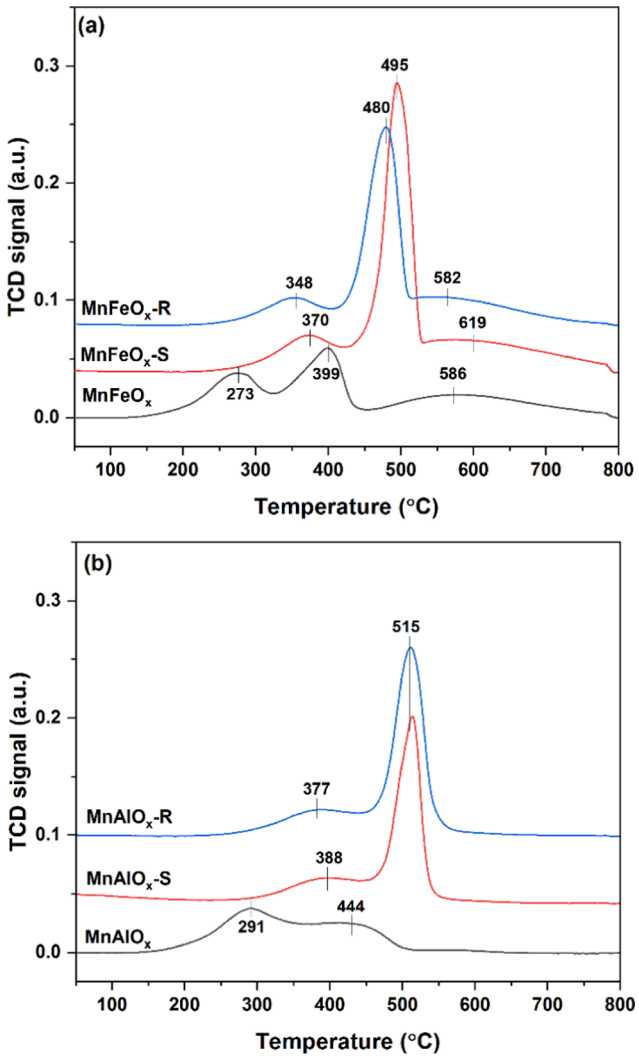

Fig. 5. H_2-TPR profiles of (a) $MnFeO_x$ and (b) $MnAlO_x$ catalysts.

2.000 ascribed to Mn^{2+} (Fig. 6a) [53], and the signal increased significantly after exposure to a reducing gas flow of NH_3/NO due to the reduction of Mn^{4+}/Mn^{3+} to Mn^{2+}. Oppositely, the signal decreased after exposure to an oxidation gas flow of O_2/NO where Mn^{2+} was re-oxidized to Mn^{4+}/Mn^{3+}, and when exposed to a full SCR gas flow of NH_3/NO/O_2 the EPR signal remained close to this oxidation curve. Thus, it is evident that a redox cycle between $Mn^{4+}/Mn^{3+}/Mn^{2+}$ existed during the SCR process and the MnO_x surface sites were mainly at high chemical states, i.e. Mn^{4+}/Mn^{3+}. The SO_2 poisoned catalyst $MnFeO_x$-S underwent similar redox changes as $MnFeO_x$ (Fig. 6b), but the signal intensity after exposure to NH_3/NO was much lower than for $MnFeO_x$, which was probably a consequence of the formed surface sulfates. Moreover, the difference in EPR intensity between the reduced/oxidized state was much smaller than for $MnFeO_x$ indicating a weaker redox ability of the MnO_x species in $MnFeO_x$-S as also found by H_2-TPR (see Section 3.5). In contrast, the difference in EPR intensity between the reduced/oxidized state of the regenerated catalyst $MnFeO_x$-R was much larger than for $MnFeO_x$-S, and the EPR intensity of the catalyst was also higher in NH_3/NO than in the full SCR feed, due to the stronger reducing environment of NH_3/NO (Fig. 6c). The latter difference was not observed with $MnFeO_x$-S, suggesting that the redox ability of MnO_x species on the catalyst was improved after regeneration in agreement with the H_2-TPR result.

For the $MnAlO_x$ catalyst only a weak EPR signal ($g_\perp$ = 2.009) assigned to Mn^{2+} was detected even when exposed to NH_3/NO (Fig. S13a), suggesting that Mn^{4+} was predominantly reduced to Mn^{3+} (EPR-silent) and only to a minor extent to Mn^{2+} when exposed to NH_3/NO. This observation agreed well with the H_2-TPR measurements (Section 3.5) where the Mn^{3+} to Mn^{2+} reduction peak of $MnAlO_x$ was less intense and shifted to higher temperature than that of $MnFeO_x$. For the SO_2 poisoned ($MnAlO_x$-S) and regenerated ($MnAlO_x$-R) catalysts, the signal of Mn^{2+} species was also detected under different gas atmospheres (Figs. S13b and c), but no significant difference in EPR intensity was observed, thus verifying that the Al-doped MnO_x catalysts indeed had a poorer redox ability than the corresponding Fe-doped catalysts.

3.8. *Mechanisms of SO_2 poisoning and regeneration of catalysts*

The formation of NH_4HSO_4 and metal sulfates are generally the two main contributors for SO_2 poisoning of SCR catalysts [54,55]. For MnO_x catalysts with excellent LT activity, the introduction of additives can increase the poisoning resistance towards SO_2 and extend the catalyst lifetime [6,7]. This is primarily attributed to a lowering of the number of active sites, mainly MnO_2, resulting from the formation of $MnSO_4$ which only decomposes at high temperature (> 800 °C). Conversely, formed NH_4HSO_4 can be decomposed at much lower temperature (< 300 °C).

When $MnFeO_x$ and $MnAlO_x$ were pretreated with SO_2 containing gas (100 ppm SO_2 + 4.5 vol% O_2, 150 °C, 6 h) both catalysts were almost completely deactivated, corresponding to a saturation of the active sites (especially MnO_x) with sulfates. As a result, the surface area of both catalysts decreased significantly and only the $MnAlO_x$ catalyst regained some of its original surface area by thermal regeneration. According to TG and XPS analysis more weakly adsorbed sulfates (mainly $Al_2(SO_4)_3$) were formed on the surface of the $MnAlO_x$ catalyst, which upon decomposition contributed to the increased surface area of the $MnAlO_x$-R catalyst, which in turn might be beneficial for the slightly increased activity of the $MnAlO_x$-R catalyst at 150 °C. However, despite its smaller surface area the $MnFeO_x$-R catalyst exhibited a much higher activity than $MnAlO_x$-R, thus corroborating other properties than the surface area led to its higher recoverability.

Fresh $MnAlO_x$ catalyst had more acid sites (0.49 mmoL/g) than $MnFeO_x$ (0.33 mmoL/g), indicating Al doping generated more acid sites than Fe doping. After SO_2 poisoning, medium-strong acid sites increased prominently on both catalysts, which could be ascribed to the formation of SO_4^{2-} on the catalyst surface resulting in the increased Brønsted acid sites, in accordance with other studies [48,51,52]. In general, the NH_3-SCR process involves the initial adsorption of NH_3 on acid sites, followed by activation through redox sites [56]. Furthermore, in LT SCR reactions, the Langmuir-Hinshelwood mechanism has been reported to have a predominant role, necessitating the adsorption of both NH_3 and NO onto the catalyst surface [6,57]. Consequently, the formation of metal sulfates not only hinders the activation of adsorbed NH_3 but also interferes with the adsorption of gaseous NO, resulting in the decreased LT SCR activity observed in both catalysts (see Fig. 2). In contrast, Brønsted acid sites have been demonstrated to be active in medium–high-temperature NH_3-SCR reaction (> 200 °C) [58], in which Eley-Rideal mechanism plays a dominant role without the need for NO adsorption on the catalyst surface, accounting for the high activity of both SO_2 poisoning catalysts at elevated temperatures (> 300 °C). After regeneration, a substantial number of acid sites remained on the catalyst surfaces due to the remaining metal sulfates. Despite this, it was evident that surface acidity was not the primary factor inducing the difference in recoverability.

Beside the activation of adsorbed NH_3, it is widely recognized that redox sites are predominantly derived from Mn sites within Mn-based oxide catalysts [59]. The swift interconversions between Mn^{4+}, Mn^{3+} and Mn^{2+} sites constitute efficient redox cycles, which in turn expedite the oxidation of NO to NO_2 thus promoting fast SCR [32]. After poisoning, the Mn^{4+} ratios in both $MnFeO_x$ and $MnAlO_x$ declined significantly, primarily due to the reduction of Mn^{4+} by SO_2. Concurrently, the O_β ratios on both catalysts also decreased upon poisoning.

Both Mn^{4+} and O_β sites are known to play critical roles in the oxidation of NO to NO_2 [60]. Therefore, the reduction in Mn^{4+} and O_β ratios could be an important contributing factor to the diminished LT activity observed in the SO_2 poisoned catalysts. However, the results from H_2-TPR indicated that the Mn sites on the $MnFeO_x$-S catalyst were more reducible compared to those on $MnAlO_x$-S. Additionally, Mn redox sites were found to be more abundant in $MnFeO_x$-S. Hence, the stronger redox ability and more Mn redox sites appeared to be the principal factors accounting for the better LT SCR activity observed in $MnFeO_x$-S (see Fig. 2).

After regeneration, the O_β ratios in both $MnFeO_x$-R and $MnAlO_x$-R increased, with $MnFeO_x$-R displaying a higher O_β ratio. Moreover, $MnFeO_x$-R exhibited a greater proportion of high-valence Mn sites (Mn^{4+}+Mn^{3+}), which are known to be active sites in the SCR reaction [32]. The higher O_β and Mn^{4+}+Mn^{3+} ratios in $MnFeO_x$-R may be attributed to electron transfer between Fe species and Mn species [17,19], which also served to weaken the interaction between Mn/Fe species with SO_4^{2-}, as evidenced by the shift in binding energy observed in Mn 2p and Fe 2p XPS signals. This finding was further supported by H_2-TPR and *in-situ* EPR, which revealed a higher content of reducible Mn species in $MnFeO_x$-R. Consequently, more active Mn species and surface-active oxygen were recovered in the Fe-doped MnO_x catalyst compared to the Al-doped counterpart through thermal regeneration. This led to the superior thermal regenerability of the Fe-doped MnO_x catalyst. In summary, the mechanisms for the SO_2 poisoning and the regeneration of the Fe- or Al-doped MnO_x catalysts can be proposed as depicted in Fig. 7.

4. Conclusions

MnO_x catalysts with Fe- and Al-doping ($MnFeO_x$ and $MnAlO_x$) were synthesized by a preferred solvothermal method and their NH_3-SCR performance, SO_2 resistance and regeneration were systematically studied. $MnFeO_x$ was found to provide better LT SCR activity than $MnAlO_x$ yielding > 90% NO_x conversion at 100–250 °C (WHSV of 240,000 mL/g•h), while $MnAlO_x$ obtained similar conversion only at temperatures of 150–250 °C. Furthermore, $MnFeO_x$ displayed enhanced tolerance to water, maintaining a NO_x conversion of 55% in the presence of 10 vol% H_2O at 185 °C, whereas $MnAlO_x$ exhibited a lower conversion of 37% under the same conditions. XPS analysis revealed that $MnFeO_x$ had a higher Mn^{4+} ratio than $MnAlO_x$, which probably promoted LT SCR by preferential oxidation of NO to NO_2. In addition, H_2-TPR and *in-situ* EPR results corroborated that MnO_x species in $MnFeO_x$ were more reducible than in $MnAlO_x$, likely due to redox reaction occurring between Mn- and Fe ions, and this further contributed to improved LT SCR performance of the catalyst.

The $MnFeO_x$ catalyst exhibited also improved SO_2 resistance and thermal regeneration compared to $MnAlO_x$. TGA in combination with SEM-EDS mapping showed that stable sulfates formed on the SO_2-poisoned catalysts $MnFeO_x$-S and $MnAlO_x$-S was a major cause of deactivation. However, XPS, H_2-TPR and *in-situ* EPR analysis revealed that $MnFeO_x$-S, and especially the thermally regenerated catalyst $MnFeO_x$-R, had higher ratios of Mn^{4+} and Mn^{3+}, more surface chemisorbed oxygen (O_β) and more favorable redox property than the analogous $MnAlO_x$ catalysts due to the electron transfer between Mn and Fe, which weakened the interactions between active sites and SO_4^{2-} and promoted the re-oxidation of Mn^{2+} to Mn^{3+}/Mn^{4+}. It overall contributed to making the $MnFeO_x$ catalyst less affected by sulfur poisoning.

In perspective, the study shed new light on improving SO_2 tolerance of MnO_x catalysts by doping MnO_x catalysts with elements that can weaken the interaction between Mn and sulfates through an appropriate treatment such as thermal regeneration.

CRediT authorship contribution statement

Huirong Li: Conceptualization, Investigation, Methodology, Formal analysis, Writing – original draft. **Leonhard Schill:** Methodology,

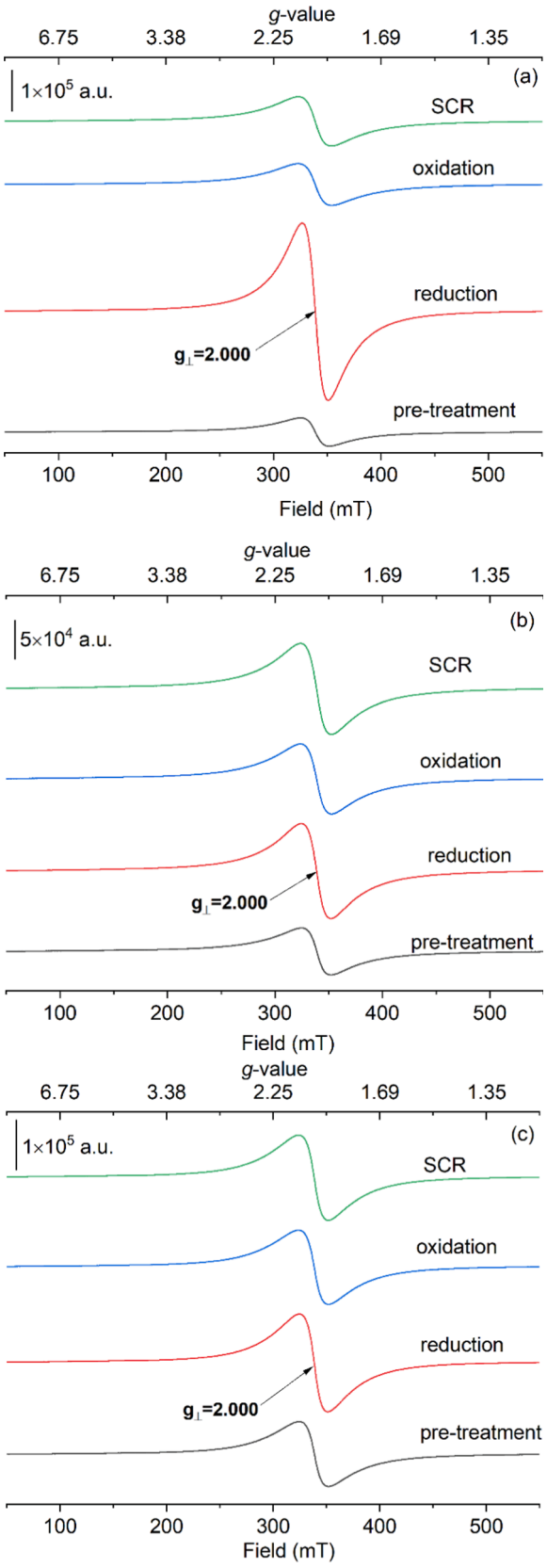

Fig. 6. *In-situ* EPR spectra of (a) $MnFeO_x$, (b) $MnFeO_x$-S and (c) $MnFeO_x$-R during exposure to different gas flows (200 mL/min) at 200 °C (pre-treatment: 10 vol% O_2/He at 250 °C for 1 h followed by cooling to 200 °C in He; reduction: 1000 ppm NO + 1000 ppm NH_3/He; oxidation: 1000 ppm NO + 10 vol% O_2/He; SCR: 1000 ppm NO + 1000 ppm NH_3 + 10 vol% O_2/He).

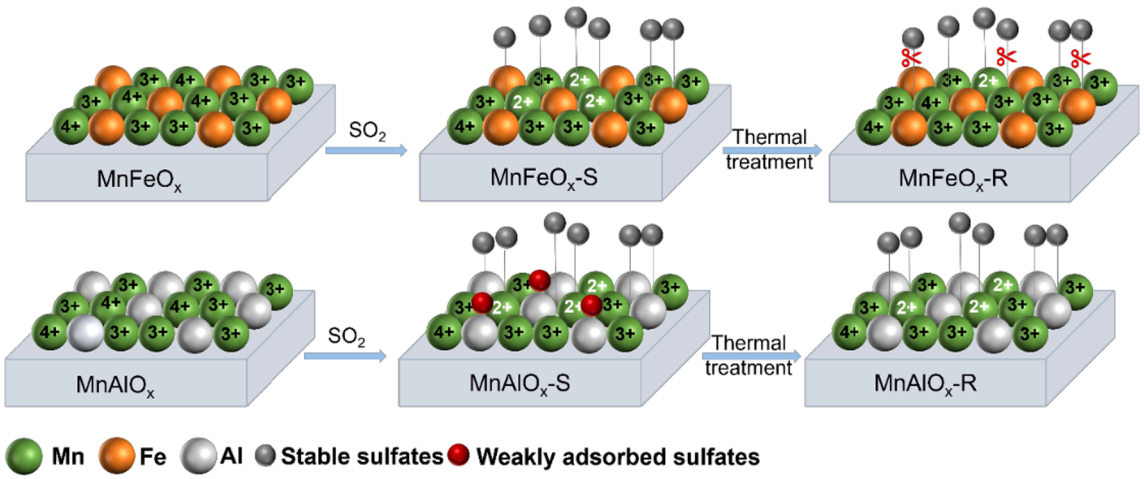

Fig. 7. Proposed mechanisms of SO_2 poisoning and regeneration of the Fe- or Al-doped MnO_x catalysts.

Writing – review & editing. **Qi Gao:** Methodology, Investigation. **Susanne Mossin:** Resources, Writing – review & editing. **Anders Riisager:** Resources, Supervision, Writing – review & editing.

Declaration of Competing Interest

The authors declare that they have no known competing financial interests or personal relationships that could have appeared to influence the work reported in this paper.

Data availability

Data will be made available on request.

Acknowledgements

H.L. thanks the China Scholarship Council (No. 202004910329) for awarding a scholarship and the Department of Chemistry, Technical University of Denmark is acknowledged for supporting the work.

Appendix A. Supplementary material

Supplementary data to this article can be found online at https://doi.org/10.1016/j.fuel.2023.130111.

References

[1] Gholami F, Tomas M, Gholami Z, Vakili M. Technologies for the nitrogen oxides reduction from flue gas: A review. Sci Total Environ 2020;714:136712.
[2] Bosch H, Janssen F. Catalytic reduction of nitrogen oxides: A review on the fundamentals and technology. Catal Today 1988;2:369–531.
[3] Roy S, Hegde MS, Madras G. Catalysis for NO_x abatement. Appl Energy 2009;86:2283–97.
[4] Chen L, Li J, Ge M. The poisoning effect of alkali metals doping over nano V_2O_5-WO_3/TiO_2 catalysts on selective catalytic reduction of NO_x by NH_3. Chem Eng J 2011;170:531–7.
[5] Shan WP, Song H. Catalysts for the selective catalytic reduction of NO_x with NH_3 at low temperature. Catal Sci Technol 2015;5:4280–8.
[6] Liu C, Shi JW, Gao C, Niu CM. Manganese oxide-based catalysts for low-temperature selective catalytic reduction of NO_x with NH_3: A review. Appl Catal A 2016;522:54–69.
[7] Xu GY, Guo XL, Cheng XX, Yu J, Fang BZ. A review of Mn-based catalysts for low-temperature NH_3-SCR: NO_x removal and H_2O/SO_2 resistance. Nanoscale 2021;13:7052–80.
[8] Meng DM, Zhan WC, Guo Y, Guo YL, Wang L, Lu GZ. A Highly effective catalyst of Sm-MnO_x for the NH_3-SCR of NO_x at low temperature: promotional role of Sm and its catalytic performance. ACS Catal 2015;5:5973–83.
[9] Shi YR, Yi HH, Gao FY, Zhao SZ, Xie ZL, Tang XL. Evolution mechanism of transition metal in NH_3-SCR reaction over Mn-based bimetallic oxide catalysts: Structure-activity relationships. J Hazard Mater 2021;413:125361.
[10] Xu Q, Fang ZL, Chen YY, Guo YL, Guo Y, Wang L, et al. Titania-Samarium-manganese composite oxide for the low-temperature selective catalytic reduction of NO with NH_3. Environ Sci Tech 2020;54:2530–8.
[11] Guo RT, Wang SX, Pan WG, Li MY, Sun P, Liu SM, et al. Different poisoning effects of K and Mg on the Mn/TiO_2 catalyst for selective catalytic reduction of NO_x with NH_3: A mechanistic study. J Phys Chem C 2017;121:7881–91.
[12] Kantcheva M. Identification, stability, and reactivity of NO_x species adsorbed on titania-supported manganese catalysts. J Catal 2001;204:479–94.
[13] Li HR, Schill L, Fehrmann R, Riisager A. Recent developments of core-shell structured catalysts for the selective catalytic reduction of NO_x with ammonia. Inorg Chem Front 2023;10:727–55.
[14] Liu Y, Zhao J, Lee JM. Conventional and new materials for selective catalytic reduction (SCR) of NO_x. ChemCatChem 2018;10:1499–511.
[15] Wu H, Liu W, Jiang X, Liang Y, Yang C, Cao J, et al. Unveiling the SO_2 resistance mechanism of a nanostructured $SiO_2(x)$@Mn catalyst for low-temperature NH_3-SCR of NO. Inorg Chem 2023;62:9971–82.
[16] Wu H, Liu W, Zhang X, Liu Q. A novel strategy for efficient utilization of manganese tailings: High SO_2 resistance SCR catalyst preparation and faujasite zeolite synthesis. Waste Manag 2023;164:66–73.
[17] Zhao F, Zhang GD, Tang ZC, Zha F. Construction of fluffy MnFe nanoparticles and their synergistic catalysis for selective catalytic reduction reaction at low temperature. Fuel 2022;322:124185.
[18] Wei L, Li X, Mu J, Wang X, Fan S, Yin Z, et al. Rationally Tailored Redox Properties of a Mesoporous Mn-Fe Spinel Nanostructure for Boosting Low-Temperature Selective Catalytic Reduction of NO_x with NH_3. ACS Sustain Chem Eng 2020;8:17727–39.
[19] Li Y, Li Y, Wang P, Hu W, Zhang S, Shi Q, et al. Low-temperature selective catalytic reduction of NO_x with NH_3 over $MnFeO_x$ nanorods. Chem Eng J 2017;330:213–22.
[20] Jin R, Liu Y, Wu Z, Wang H, Gu T. Low-temperature selective catalytic reduction of NO with NH_3 over MnCe oxides supported on TiO_2 and Al_2O_3: A comparative study. Chemosphere 2010;78:1160–6.
[21] Yao X, Kong T, Yu S, Li L, Yang F, Dong L. Influence of different supports on the physicochemical properties and denitration performance of the supported Mn-based catalysts for NH_3-SCR at low temperature. Appl Surf Sci 2017;402:208–17.
[22] Fan ZY, Shi JW, Niu CH, Wang BR, He C, Cheng YH. The insight into the role of Al_2O_3 in promoting the SO_2 tolerance of MnO_x for low-temperature selective catalytic reduction of NO_x with NH_3. Chem Eng J 2020;398:125572.
[23] France LJ, Yang Q, Li W, Chen ZH, Guang JY, Guo DW, et al. Ceria modified $FeMnO_x$-Enhanced performance and sulphur resistance for low-temperature SCR of NO_x. Appl Catal B: Environ 2017;206:203–15.
[24] Wang Y, Yi W, Yu J, Zeng J, Chang H. Novel methods for assessing the SO_2 poisoning effect and thermal regeneration Possibility of MO_x–WO_3/TiO_2 (M = Fe, Mn, Cu, and V) catalysts for NH_3-SCR. Environ Sci Tech 2020;54:12612–20.
[25] Mu J, Li X, Wang X, Fan S, Yin Z, Li Z, et al. New insight into the effects of NH_3 on SO_2 poisoning for in situ removal of metal sulfates in low-temperature NH_3-SCR over an Fe-V catalyst. J Phys Chem C 2020;124:21396–406.
[26] Putluru SSR, Schill L, Jensen AD, Siret B, Tabaries F, Fehrmann R. Mn/TiO_2 and Mn-Fe/TiO_2 catalysts synthesized by deposition precipitation-promising for selective catalytic reduction of NO with NH_3 at low temperatures. Appl Catal B: Environ 2015;165:628–35.
[27] Huang XS, Dong F, Zhang GD, Guo Y, Tang ZC. A strategy for constructing highly efficient yolk-shell Ce@Mn@TiO_x catalyst with dual active sites for low-temperature selective catalytic reduction of NO with NH_3. Chem Eng J 2021;419:129572.
[28] Zhang L, Du TY, Qu HX, Chi B, Zhong Q. Synthesis of Fe-ZSM-5@Ce/mesoporous-silica and its enhanced activity by sequential reaction process for NH_3-SCR. Chem Eng J 2017;313:702–10.
[29] Tounsi H, Djemal S, Petitto C, Delahay G. Copper loaded hydroxyapatite catalyst for selective catalytic reduction of nitric oxide with ammonia. Appl Catal B: Environ 2011;107:158–63.

[30] Yang S, Xiong S, Liao Y, Xiao X, Qi F, Peng Y, et al. Mechanism of N_2O formation during the low-temperature selective catalytic reduction of NO with NH_3 over Mn-Fe spinel. Environ Sci Technol 2014;48:10354–62.
[31] An DQ, Yang S, Zou WX, Sun JF, Tan W, Ji JW, et al. Unraveling the SO_2 poisoning effect over the lifetime of MeO_x (Me = Ce, Fe, Mn) catalysts in low-temperature NH_3-SCR: interaction of reaction atmosphere with surface species. J Phys Chem C 2022;126:12168–77.
[32] Fang D, Xie J, Hu H, Yang H, He F, Fu Z. Identification of MnO_x species and Mn valence states in MnO_x/TiO_2 catalysts for low temperature SCR. Chem Eng J 2015; 271:23–30.
[33] Li J, Chen J, Ke R, Luo C, Hao J. Effects of precursors on the surface Mn species and the activities for NO reduction over MnO_x/TiO_2 catalysts. Catal Commun 2007;8: 1896–900.
[34] Cai Z, Zhang G, Tang Z, Zhang J. MnFe@CeO_x Core-Shell nanocages for the selective catalytic reduction of NO with NH_3 at low temperature. ACS Appl Nano Mater 2022;5:3619–31.
[35] Jin T, Yamaguchi T, Tanabe K. Mechanism of acidity generation on sulfur-promoted metal oxides. J Phys Chem C 1986;90:4794–6.
[36] Furuta S, Matsuhashi H, Arata K. Catalytic action of sulfated tin oxide for etherification and esterification in comparison with sulfated zirconia. Appl Catal A 2004;269:187–91.
[37] Chen L, Zhang C, Li YX, Chang CR, He C, Lu Q, et al. Hierarchically hollow MnO_2@ CeO_2 heterostructures for NO oxidation: remarkably promoted activity and SO_2 tolerance. ACS Catal 2021;11:10988–96.
[38] Gao FY, Tang XL, Yi HH, Li JY, Zhao SZ, Wang JG, et al. Promotional mechanisms of activity and SO_2 tolerance of Co- or Ni-doped MnO_x-CeO_2 catalysts for SCR of NO_x with NH_3 at low temperature. Chem Eng J 2017;317:20–31.
[39] Chen Z, Ren S, Wang M, Yang J, Chen L, Liu W, et al. Insights into samarium doping effects on catalytic activity and SO_2 tolerance of $MnFeO_x$ catalyst for low-temperature NH_3-SCR reaction. Fuel 2022;321:124113.
[40] Karami A, Salehi V. The influence of chromium substitution on an iron-titanium catalyst used in the selective catalytic reduction of NO. J Catal 2012;292:32–43.
[41] Zhang JL, Tian H, Yu YK, Jiang ZY, Ma MD, He C. Novel CuO@TiO_2 core-shell nanostructure catalyst for selective catalytic reduction of NO_x with NH_3. Catal Lett 2021;151:2502–12.
[42] Sun P, Guo R, Liu S, Wang S, Pan W, Li M. The enhanced performance of MnO_x catalyst for NH_3-SCR reaction by the modification with Eu. Appl Catal A 2017;531: 129–38.
[43] Fang X, Liu YJ, Cheng Y, Cen WL. Mechanism of Ce-modified birnessite-MnO_2 in promoting SO_2 poisoning resistance for low-temperature NH_3-SCR. ACS Catal 2021;11:4125–35.
[44] Lin HF, Zhao SY, Li JT, Yao ZTA, Li CM, Gaoa SQ, et al. The effect of SO_2 on the structural evolution of a supported $Mn_2V_2O_7$ catalyst and its DeNO_x performance. Catal Sci Technol 2021;11:5598–605.
[45] Shi YR, Yi HH, Gao FY, Zhao SZ, Xie ZL, Tang XL. Facile synthesis of hollow nanotube $MnCoO_x$ catalyst with superior resistance to SO_2 and alkali metal poisons for NH_3-SCR removal of NO_x. Sep Purif Technol 2021;265:118517.
[46] Zhang QL, Zhang YQ, Zhang TX, Wang HM, Ma YP, Wang JF, et al. Influence of preparation methods on iron-tungsten composite catalyst for NH_3-SCR of NO: The active sites and reaction mechanism. Appl Surf Sci 2020;503:144190.
[47] Kwon DW, Kim DH, Lee S, Kim J, Ha HP. A dual catalytic strategy by the nature of the functionalization effect as well as active species on vanadium-based catalyst for enhanced low temperature SCR. Appl Catal B: Environ 2021;289:120032.
[48] Xu LW, Wang CZ, Chang HZ, Wu QR, Zhang T, Li JH. New insight into SO_2 poisoning and regeneration of CeO_2-WO_3/TiO_2 and V_2O_5-WO_3/TiO_2 catalysts for low-temperature NH_3-SCR. Environ Sci Technol 2018;52:7064–71.
[49] Li HR, Miao JF, Su QF, Yu YK, Chen YT, Chen JS, et al. Improvement in alkali metal resistance of commercial V_2O_5-WO_3/TiO_2 SCR catalysts modified by Ce and Cu. J Mater Sci 2019;54:14707–19.
[50] Yan R, Lin SX, Li YL, Liu WM, Mi YY, Tang CJ, et al. Novel shielding and synergy effects of Mn-Ce oxides confined in mesoporous zeolite for low temperature selective catalytic reduction of NO_x with enhanced SO_2/H_2O tolerance. J Hazard Mater 2020;396:122592.
[51] Yu Y, Miao J, He C, Chen J, Li C, Douthwaite M. The remarkable promotional effect of SO_2 on Pb-poisoned V_2O_5-WO_3/TiO_2 catalysts: An in-depth experimental and theoretical study. Chem Eng J 2018;338:191–201.
[52] Lee T, Bai H. Metal sulfate poisoning effects over $MnFe/TiO_2$ for selective catalytic reduction of NO by NH_3 at low temperature. Ind Eng Chem Res 2018;57:4848–58.
[53] Vuong TH, Bartling S, Bentrup U, Lund H, Rabeah J, Atia H, et al. Synergistic effect of VO_x and MnO_x surface species for improved performance of $V_2O_5/Ce_{0.5}Ti_{0.5-x}Mn_xO_{2-\delta}$ catalysts in low-temperature NH_3-SCR of NO. Catal Sci Technol 2018;8:6360–74.
[54] Liu CX, Wang HJ, Zhang ZY, Liu QL. The latest research progress of NH_3-SCR in the SO_2 resistance of the catalyst in low temperatures for selective catalytic reduction of NO_x. Catalysts 2020;10:1034.
[55] Damma D, Ettireddy PR, Reddy BM, Smirniotis PG. A Review of low temperature NH_3-SCR for removal of NO_x. Catalysts 2019;9:349.
[56] Han LP, Cai SX, Gao M, Hasegawa J, Wang PL, Zhang JP, et al. Selective catalytic reduction of NO_x with NH_3 by using novel catalysts: state of the art and future prospects. Chem Rev 2019;119:10916–76.
[57] Yang SJ, Wang CZ, Li JH, Yan NQ, Ma L, Chang HZ. Low temperature selective catalytic reduction of NO with NH_3 over Mn-Fe spinel: Performance, mechanism and kinetic study. Appl Catal B: Environ 2011;110:71–80.
[58] Xie RY, Ma L, Li ZH, Qu Z, Yan NQ, Li JH. Review of sulfur promotion effects on metal oxide catalysts for NO_x emission control. ACS Catal 2021;11:13119–39.
[59] Kumar MS, Alphin MS, Manigandan S, Vignesh S, Vigneshwaran S, Subash T. A review of comparison between the traditional catalyst and zeolite catalyst for ammonia-selective catalytic reduction of NO_x. Fuel 2023;344:128125.
[60] Qi ZY, Chen B, Man BC, Li ZW, Feng K, Yan BH, et al. Unraveling the contribution of valence state to the NO oxidation activity of manganese oxides. Chem Eng J 2023;462:142173.